J. Phys. A: Math. Gen. **33** (2000) 1055–1064. Printed in the UK PII: S0305-4470(00)02023-0

Bifurcations of beam–beam like maps

C Polymilis†, Ch Skokos†, G Kollias†, G Servizi‡ and G Turchetti‡

† Department of Physics, University of Athens, Panepistemiopolis, 15784 Zografos, Greece
‡ Dipartimento di Fisica della Università di Bologna, Italy, INFN Sezione di Bologna, Italy

Received 18 February 1999, in final form 29 October 1999

Abstract. The bifurcations of a class of mappings including the beam–beam map are examined. These maps are asymptotically linear at infinity where they exhibit invariant curves and elliptic periodic points. The dynamical behaviour is radically different with respect to the Hénon-like polynomial maps whose stability boundary (dynamic aperture) is at a finite distance. Rather than the period-doubling bifurcations exhibited by the Hénon-like maps, we observe a systematic appearance of tangent bifurcations and in phase space one observes the disappearance of chains of islands born from the origin and coming from infinity. This behaviour has relevant consequences on the transport process.

1. Introduction

Area-preserving maps have been extensively investigated since they capture the generic properties of the Poincaré map of a Hamiltonian system with two degrees of freedom. The standard map describes the magnetic field lines of a plasma and is obtained by perturbing an anisochronous integrable system. The Hénon map [1], defined as the quadratic perturbation of a linear map, is the simplest model of a particle accelerator [2]. Denoting x as the horizontal coordinate and y as the conjugate momentum, the Hénon map, to which any other quadratic map is reducible after a linear transformation, reads

$$\begin{pmatrix} x' \\ y' \end{pmatrix} = \mathsf{R}(2\pi\nu) \begin{pmatrix} x \\ y + x^2 \end{pmatrix}. \tag{1}$$

This map gives the consequences, on the Poincaré section, of the orbit followed by a charged particle moving in a linear lattice with a thin sextupole. The fixed point corresponds to the closed orbit and x, y are the normalized Courant–Sneyder coordinates scaled by $\beta^{3/2}$. We recall that $\beta^{1/2}$ is the amplitude of the beam for unit emittance, defined as $(4\pi)^{-1}$ times the area of the phase-space ellipse filled by the particles.

The quadratic nonlinearity determines the usual pattern of invariant curves, chains of islands and chaotic layers in the neighbourhood of the fixed point and the existence of a finite-stability basin, whose border is known as the *dynamic aperture*. In the inner part of the stability region the map has a quasi-integrable behaviour and its orbits can be interpolated by the level lines of Hamiltonians obtained via normal forms [2, 3].

The maps where the quadratic nonlinearity is replaced by a bounded nonlinearity, vanishing quadratically at the origin, exhibit a different dynamical behaviour. In the normalized coordinates the map is given by (1), where x^2 is replaced by $\beta^{1/2} f(\beta^{1/2} x)$. Unlike the quadratic map, the β factor cannot be scaled. In this paper we investigate the dynamical behaviour and

0305-4470/00/051055+10$30.00

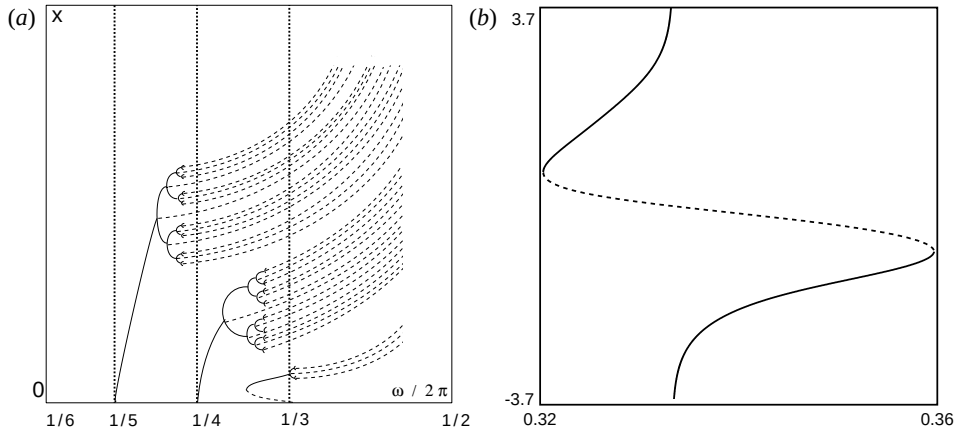

Figure 1. (*a*) Sketch of the bifurcation diagrams in the ν, x plane for the resonances $\frac{1}{5}$, $\frac{1}{4}$, $\frac{1}{3}$ of Hénon-like maps. (*b*) Bifurcation diagram for the resonance $\frac{1}{3}$ of the beam–beam map. Continuous and dashed curves denote stable and unstable periodic points, respectively.

the bifurcation pattern in the linear frequency ν, by choosing $\beta = 1$. The dependence on β in the beam–beam map corresponding to a Gaussian nonlinearity is briefly outlined.

The dynamical properties and the bifurcation patterns have been investigated for other quadratic maps [4, 5] depending on a parameter μ. These maps can be transformed into (1) with a translation and/or a similarity transformation (see the appendix). In both cases $\nu \in [0, \frac{1}{2}]$ is a smooth invertible function of μ, but the similarity transformation is singular at $\nu = 0$. The characteristic diagram of (1) in the linear frequency ν has been recently investigated [6]. It was shown that all the resonance curves in the ν, x plane, issued from the main family $x = 0$ at any rational $\nu = p/q$, undergo a sequence of period-doubling bifurcations at $\nu = \nu_n$, satisfying the Feigenbaum scaling laws, with a ratio of two subsequent interval lengths $\delta_n = (\nu_{n+1} - \nu_n)/(\nu_n - \nu_{n-1})$ approaching the same universal value found in other conservative systems [7]. For each family the stable branches approach a finite value of ν in the frequency range $[0, \frac{1}{2}]$, whereas the unstable branches always seem to approach the end point $\nu = \frac{1}{2}$ asymptotically when $x \to \infty$ (see the sketch in figure 1(*a*)). This result is found since the distance of the chains of islands remains bounded whereas the hyperbolic points migrate to infinity, as confirmed by inspection of the hyperbolic manifolds which extend further and further away before returning to undergo homoclinic and heteroclinic intersections. Higher-order bifurcations having similar features are observed starting from any of the daughter families, which now play the role of the main family and the story repeats self-similarly *ad infinitum*. The resonance $\frac{1}{3}$ has a different behaviour since the unstable branch born at the origin extends for $\nu < \frac{1}{3}$ until a tangent bifurcation occurs (see figure 1(*a*)); the stable branch bends back to reach $\nu = \frac{1}{3}$ at a finite distance from the origin, where it undergoes a period-doubling bifurcation with the unstable branches tending to infinity as $\nu \to \frac{1}{2}$ (see [6] and references therein). This anomalous behaviour occurs since in a small interval below $\nu = \frac{1}{3}$ the rotation number increases with the distance from the origin.

The bounded maps, having invariant curves near the origin and at infinity present new bifurcation scenarios and an increase of chaoticity in the intermediate region, which can be explained by the behaviour of the asymptotic curves.

2. Bounded maps

A new scenario emerges when the phase space is not compact but the origin and infinity are surrounded by invariant curves. This occurs when the quadratic nonlinearity of the Hénon map is replaced by an algebraic or transcendental function which vanishes quadratically at the origin and has a constant limit at infinity. A model with such features is the beam–beam map, which describes the interaction of a particle of a dilute beam with the charge of an intense beam having a Gaussian distribution in the absence of lattice nonlinearities [8]

$$\begin{pmatrix} x' \\ y' \end{pmatrix} = \mathsf{R}(2\pi\nu) \begin{pmatrix} x \\ y + 1 - \mathrm{e}^{-x^2} \end{pmatrix} \tag{2}$$

where $\mathsf{R}(\alpha)$ denotes the rotation matrix of angle α. The distribution of the fixed points for area preserving maps with bounded nonlinearities has been previously investigated [9], but the linear transformation which brings these maps to the standard form (1) is singular at $\nu = 0$ and the nonlinearity has a dependence on ν which cannot be scaled out. The numerical investigation of the bifurcation pattern of the map (2) when ν is varied continuously is new and physically relevant since it allows one to understand the dynamics of the beam–beam-like maps. When we move to infinity along any straight line different from the y-axis, the map approaches the linear map given by $\mathsf{R}(2\pi\nu)$ composed of the unit translation along the y-axis. Such a map is a rotation about the fixed point $x = \frac{1}{2}\cot(\pi\nu)$, $y = \frac{1}{2}$. It is, therefore, not surprising to observe invariant curves by approaching the origin and also at large distances from it. In this case period-doubling bifurcations are not observed (up to a resonance p/q, with $q \leqslant 10$), whereas tangent bifurcations appear systematically. The behaviour of odd and even resonances (up to the order we have examined) is different, the latter being much simpler. All the resonances are born at the origin and appear simultaneously at infinity and their stable and unstable branches collide via tangent bifurcations. In this case the phase space where two or more islands of the same resonant order p/q are present, cannot be described by an autonomous interpolating Hamiltonian. In spite of the fact that maps (1) and (2) agree up to quadratic terms approaching the origin the same daughter families may exhibit different behaviour (see the discussion of resonances belonging to the Farey tree $[\frac{4}{13}, \frac{7}{22}]$ in [5]). The scenario described with two or more tangent bifurcations is not a peculiarity of the beam–beam map but seems to be typical of maps bounded at infinity and approaching the Hénon map at the origin.

The one-turn map of a particle moving in a linear lattice with a localized nonlinear force $f(x)$, vanishing as x^2 for $x \to 0$, is given by

$$\begin{pmatrix} \xi' \\ \dot{\xi}' \end{pmatrix} = \mathsf{L} \begin{pmatrix} \xi \\ \dot{\xi} + f(\xi) \end{pmatrix} \tag{3}$$

where ξ is the horizontal coordinate and $\dot{\xi} \equiv \mathrm{d}\xi/\mathrm{d}s$ is its derivative with respect to the arc length. Assuming the orbit to be closed we have $\mathrm{Tr}\,\mathsf{L} = 2\cos(2\pi\nu)$ and the unimodular matrix L is conjugated to a rotation

$$\mathsf{L} = \mathsf{V}\mathsf{R}(2\pi\nu)\mathsf{V}^{-1} \qquad \mathsf{V} = \begin{pmatrix} \beta^{1/2} & 0 \\ -\alpha\beta^{-1/2} & \beta^{-1/2} \end{pmatrix}. \tag{4}$$

The new coordinates x, y are obtained with the linear transformation V^{-1}, and the scaling $\beta^{3/2}$ and the one-turn map becomes

$$\begin{pmatrix} x' \\ y' \end{pmatrix} = \mathsf{R}(2\pi\nu) \begin{pmatrix} x \\ y + \beta^2 f\left(\frac{x}{\beta}\right) \end{pmatrix} \qquad \begin{pmatrix} x \\ y \end{pmatrix} = \beta^{3/2}\mathsf{V}^{-1} \begin{pmatrix} \xi \\ \dot{\xi} \end{pmatrix}. \tag{5}$$

For a quadratic nonlinearity $f(x) = x^2$, the map becomes exactly the Hénon map. If $f(x)$ is any nonlinear function the β dependence does not scale out. We have also examined the

Table 1. Tangent bifurcation values for resonances $\frac{1}{4}$ (left) and $\frac{1}{5}$ (right).

		ν_{-1}	0.199 87
ν_0	0.250 00	ν_0	0.200 00
ν_1	0.252 49	ν_1	0.206 42
ν_2	0.267 08	ν_2	0.210 94
		ν_3	0.213 33
		ν_4	0.215 02

dependence on β of the beam–beam map, where $f(x) = 1 - \mathrm{e}^{-x^2}$, and for an algebraic map where $f(x) = x^2/(1 + x^2)$ has the same behaviour at the origin and approaches the same constant value at infinity. The maps we have considered explicitly read

$$\begin{pmatrix} x' \\ y' \end{pmatrix} = \mathsf{R}(2\pi\nu) \begin{pmatrix} x \\ y + \beta^2(1 - \mathrm{e}^{-x^2/\beta^2}) \end{pmatrix} \tag{6a}$$

$$\begin{pmatrix} x' \\ y' \end{pmatrix} = \mathsf{R}(2\pi\nu) \begin{pmatrix} x \\ y + \frac{x^2}{1+x^2/\beta^2} \end{pmatrix} \tag{6b}$$

and both exhibit the Hénon bifurcation scenarios for large values of β and the beam–beam map (2) bifurcation scenarios for $\beta^2 < 2$ (notice that in the limit $\beta \to 0$ the region of nonlinear orbits in phase space shrinks to zero since the linear map is recovered). For intermediate values of β more complex structures appear.

3. Numerical investigation

Having obtained numerical evidence that the beam–beam bifurcation patterns are not a peculiarity of this map but are typical of maps approaching the Hénon map at the origin and a linear map at infinity, it is worthwhile describing them in more detail by inspecting the characteristics diagram and some phase portraits. These diagrams are usually constructed by drawing the characteristic curve corresponding to a single fixed point of a resonance. In the present case, the standard procedure cannot be used because of the complexity of the patterns. As a consequence, we draw as many curves as we need to resolve it. The numerical investigation was carried out by using two graphically interactive codes: DYNAMICS [10] and GIOTTO [11].

In order to illustrate higher-order resonances we denote by S, U the stable and unstable families of fixed points, respectively.

The resonance $\frac{1}{4}$ has a stable branch (Sa1) issued at the origin $x = 0$ for $\nu = \frac{1}{4}$, which extends to higher values of ν until a tangent bifurcation occurs at ν_1 (see table 1) and the unstable branch (Ub1) bends and asymptotically reaches $\nu = \frac{1}{4}$ at infinite distance from the origin (see figure 2(*a*)). A similar pattern is observed for the unstable branch issued from the origin (Ua1), which becomes stable (Sb1) after a tangent bifurcation occurring at $\nu_2 > \nu_1$. The stability index $\alpha(\nu) = \frac{1}{2}\,\mathrm{Tr}\,|M'|$ (where $M'(x, y)$ denotes the tangent map evaluated at the fixed point $x = x(\nu)$, $y = y(\nu)$) of each family, is not monotonic, as for the Hénon map, and has a unique minimum (see figure 2(*b*)). As a consequence, the second-order resonances correspond to the same Farey tree, a necessary condition for the creation of bubbles [11–13]. In order to have a better understanding of the topological changes occurring when ν varies in figure 3 we show the phase portraits of the map when ν approaches the tangent bifurcation values. In figure 3(*a*) corresponding to $\nu = 0.251 < \nu_1$ two chains of four islands are observed. The hyperbolic and elliptic points of the inner chain are close to merge and disappear through a tangent bifurcation as shown in figure 3(*b*) corresponding to $\nu = 0.253 > \nu_1$. In figure 3(*c*),

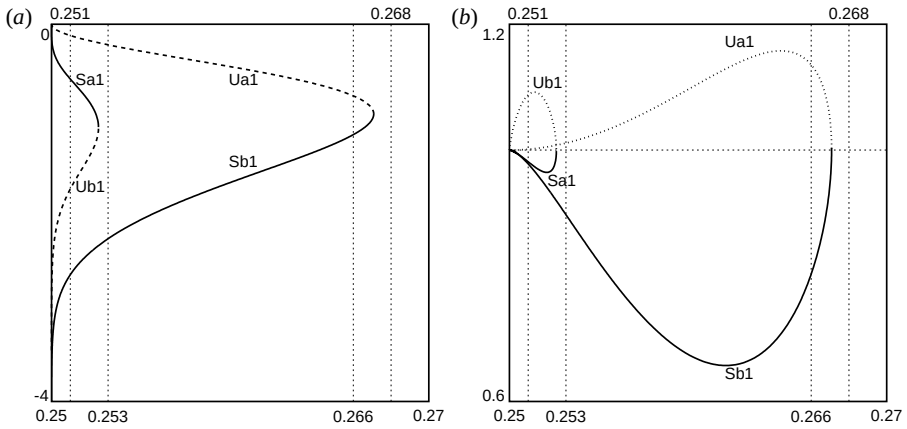

Figure 2. (*a*) Characteristic diagram in the ν, x plane for the $\nu = \frac{1}{4}$ resonance. (*b*) Stability diagram in the ν, α plane where 2α is the modulus of the trace of the tangent map. The dotted vertical lines correspond to the values of ν at which the phase plots are shown in figure 3.

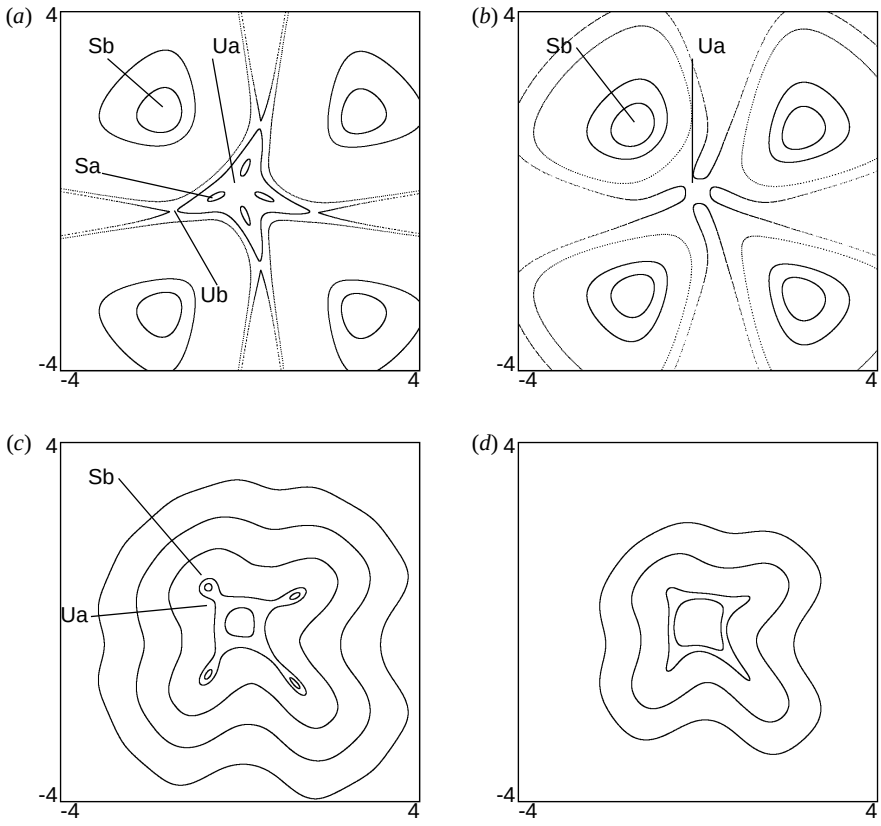

Figure 3. Phase portraits of the beam–beam map for the values of ν selected in figure 2 to illustrate the bifurcations of the resonance $\frac{1}{4}$: (*a*) $\nu = 0.251$, (*b*) $\nu = 0.253$, (*c*) $\nu = 0.266$, (*d*) $\nu = 0.268$.

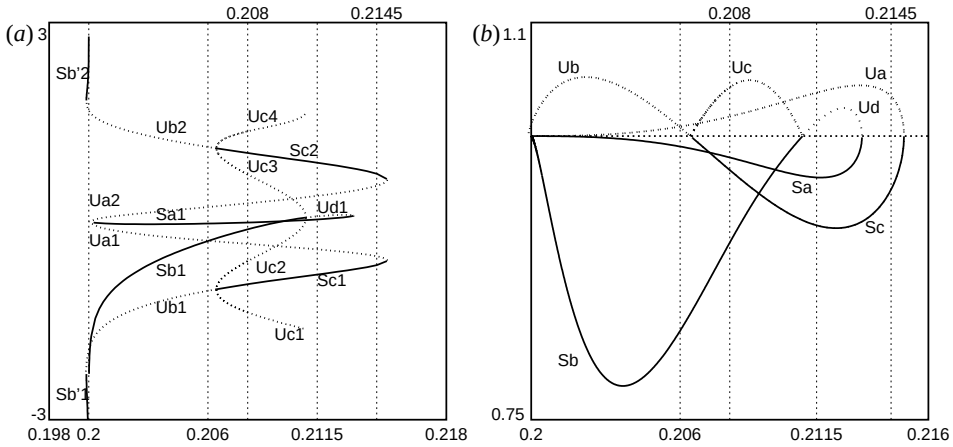

Figure 4. The same as figure 2 for the resonance $\frac{1}{5}$. The two extra trajectories drawn for the periodic points coming from infinity are denoted with the number 2. The dotted vertical lines correspond to the values of ν at which the phase plots are shown in figure 5.

corresponding to $\nu = 0.266 < \nu_2$, the elliptic and hyperbolic points of the surviving chain have come close to each other and disappear via a new tangent bifurcation at ν_2 as shown in figure 3(*d*), corresponding to $\nu = 0.268 > \nu_2$ (see table 1).

The resonances $\frac{1}{6}$, $\frac{1}{8}$ have the same behaviour as $\frac{1}{4}$.

Concerning the odd resonances, we first discuss the behaviour of $\nu = \frac{1}{3}$. The resonance $\frac{1}{3}$, born at the origin for $\nu = \frac{1}{3}$, is unstable. This unstable branch extends in a finite interval, at the ends of which two tangent bifurcations occur and the emerging stable branches reach $\nu = \frac{1}{3}$, again from above and below asymptotically at infinite distance from the origin (see figure 1(*b*)).

The higher-order odd resonances have a similar behaviour and we discuss $\nu = \frac{1}{5}$. We follow three of the ten characteristic curves born from the origin at $\nu = \frac{1}{5}$: one stable (Sa1) and two unstable (Ua1, Ua2). The branch (Sa1) becomes unstable (Ud1) at ν_3 (see table 1) after a tangent bifurcation and again interchanges its stability becoming (Sb1) at a value ν_2 lower than ν_3, and remains stable up to infinity (see figure 4). The two unstable branches (Ua1), (Ua2) become stable (Sc1), (Sc2) after a tangent bifurcation at $\nu_4 > \nu_3$. These branches interchange their stability at a value $\nu_1 < \nu_2$. These unstable branches (Ub1), (Ub2) persist until a value $\nu_{-1} < \frac{1}{5}$, then interchange stability becoming (Sb′1), (Sb′2) after a tangent bifurcation and tend to $\nu = \frac{1}{5}$ from below at infinite distance from the origin. At the values, ν_2 and ν_1, where the stability interchange occurs a new family (Uc) is born. Since the stability index at ν_2 and ν_1 is equal to +1, the new family (Uc) has the same multiplicity of five as its mother family. As for even resonances, the curves $\alpha(\nu)$ representing the stability index in the region $\alpha < 1$ have minima at different values of ν, and the same considerations hold concerning the corresponding Farey trees.

For some values of ν, marked with dotted curves in figure 4(*a*), the phase portraits are shown in figure 5, to illustrate the changes occurring in the topology of the orbits. Starting from $\nu = 0.199\,98$ we have a chain of five islands shown in figure 5(*a*). As $\nu \to \frac{1}{5}$, the elliptic points move to infinity, while the hyperbolic points remain at a finite distance. For $\nu = 0.206 > \frac{1}{5}$, the hyperbolic points (Ub) are still present and elliptic points (Sb) appear from infinity to form the exterior chain of islands shown in figure 5(*b*), where an inner chain of islands ((Sa), (Ua))

born from the origin at $\nu = \frac{1}{5}$, is present. The unstable point (Ub1) becomes stable (Sc1) and two hyperbolic points (Uc1), (Uc2) appear in figure 5(*c*) corresponding to $\nu = 0.208$; the inner chain and the outer elliptic points (Sb) remain. Two of these hyperbolic points (Uc2), (Uc3) collide with the outer elliptic point (Sb1) generating a new hyperbolic point (Ud1) and in figure 5(*d*) we show the orbits for $\nu = 0.2115$ after the collision. In figure 5(*e*) only one chain of islands consisting of previous outer elliptic points (Sc) and inner hyperbolic points (Ua) remains.

The same behaviour was found for the following resonances: $\frac{2}{5}$, $\frac{1}{7}$, $\frac{2}{7}$, $\frac{3}{7}$, $\frac{1}{9}$, $\frac{2}{9}$, $\frac{4}{9}$, and also for the even resonance $\frac{3}{8}$.

To conclude the present analysis we summarize the results on the parametric map (6*a*). For small values of β the resonances close to the origin undergo period-doubling bifurcations, as in the Hénon map, without being affected by the presence of the other distant families. When β increases the Hénon chain interacts with the families coming from infinity and complicated bifurcations appear. At the same time a couple of periodic points move from infinity on a straight line towards the origin until they are annihilated by a tangent bifurcation. This scenario can be easily verified for resonance $\frac{1}{4}$ or other even resonances. For the rational map (6*b*) resonances $\nu = \frac{1}{3}$, $\frac{1}{4}$, $\frac{1}{6}$ follow the scenario found in the parametric beam–beam map (6*a*).

Conclusions

We have proposed a new family of non-polynomial maps with a linear behaviour at infinity and approaching the Hénon map at the origin. These maps have a different dynamical behaviour which clearly emerges from the numerical bifurcation analysis. The analytical description would require at least two different interpolating Hamiltonians to obtain an integrable approximation of the orbits in the neighbourhood of the origin and infinity. For the Hénon map a single interpolation of the orbits in the stability basin is sufficient, while for the present case the interpolation in the neighbourhood of infinity remains an open problem just as the application of the KAM theory to prove the existence of invariant curves at very large distance from the origin.

The present analysis is certainly not exhaustive but sheds some light on the basic mechanisms occurring in this class, which is not only relevant in beam dynamics but more generally, for Hamiltonian systems. The main feature emerging from this analysis is the systematic appearance of tangent bifurcations [13, 14] and it is well known that they are connected with the disappearance or appearance of periodic orbits. We found that the odd resonances appear for values lower than $\nu = p/q$ at which they are born from the main family, a phenomenon that is only observed for the resonance $\frac{1}{3}$ for Hénon-like maps. The characteristic of $\frac{1}{3}$ intersects the characteristic of the main family obliquely [15, 16] but all other resonances bifurcate directly. In the present case the tangent bifurcations occur above and below p/q, whereas for the Hénon map it occurs at a value $\nu < \frac{1}{3}$.

When q is even the tangent bifurcations only occur for $\nu > p/q$. It is worthwhile noting that up to order $q = 10$ no period-doubling bifurcations are observed. In this respect the map is quite different from the Hénon map where the period-doubling bifurcations appear systematically.

The curves corresponding to the stability index of both even and odd resonances have minima below +1, a condition allowing the presence of bubbles.

We expect that the intersection of the homoclinic tangles issued from the manifolds of the unstable periodic points which forms heteroclinic tangles is completely different with respect

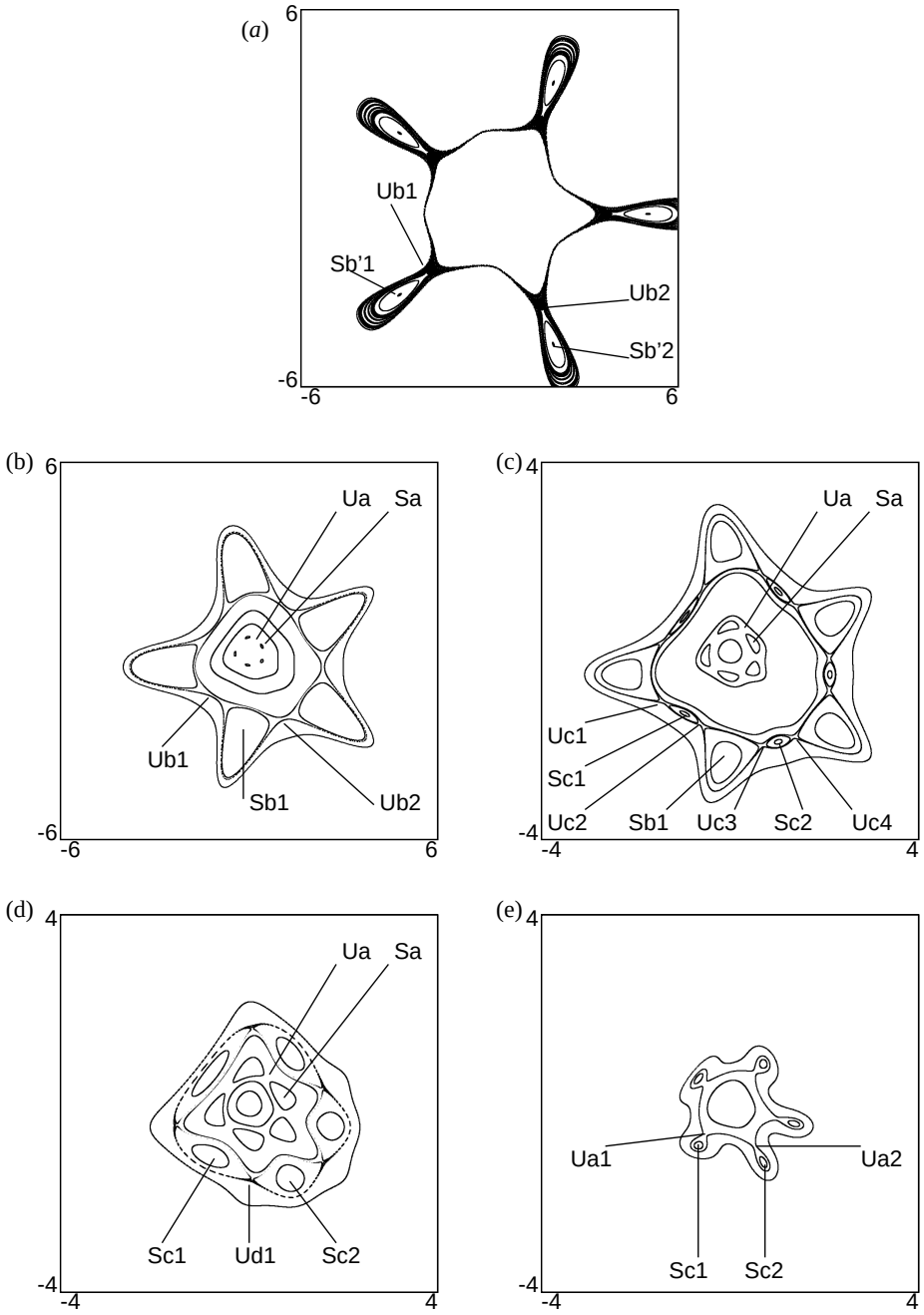

Figure 5. Phase portraits of the beam–beam map for the values of ν selected in figure 4 to illustrate the bifurcations of the resonance $\frac{1}{5}$. (*a*) $\nu = 0.199\,98$, (*b*) $\nu = 0.206$, (*c*) $\nu = 0.208$, (*d*) $\nu = 0.2115$, (*e*) $\nu = 0.2145$.

to the Hénon-like map. Indeed, for map (1) the lobes get further and further away from the origin in agreement with the existence of hyperbolic points whose characteristics extend to

infinity, whereas for map (2) these tangles are confined in a bounded region delimited by invariant curves. On the other hand, the dynamical behaviour of the homoclinic tangles is different, depending on whether the phase space is compact or not [17], and thus the transport mechanisms will be different. A more detailed investigation of these chaotic regions would allow the study of the diffusion, whereas an extension to 4D maps would be desirable.

Appendix

Bountis map

The quadratic map considered in [5] is given by

$$\begin{aligned} x' &= 1 - y + ax^2 \\ y' &= x \end{aligned} \tag{A1}$$

and its fixed points are $\boldsymbol{x}_1 = (\frac{1}{2}, \frac{1}{2})$ and $\boldsymbol{x}_2 = (\frac{2}{a}, \frac{2}{a})$. The first one is elliptic as long as $-3 \leqslant a \leqslant 1$, and the eigenvalues are $\mathrm{e}^{\pm \mathrm{i}2\pi\nu}$, where $\cos(2\pi\omega) = 1 - (1-a)^{1/2}$. After a translation, which brings $\boldsymbol{x}_1$ into the origin, the linear part L is transformed into a rotation by a similarity unimodular transformation

$$\begin{aligned} \mathsf{L} &\equiv \begin{pmatrix} 2\cos(2\pi\nu) & -1 \\ 1 & 0 \end{pmatrix} = \mathsf{V}\mathsf{R}(2\pi\nu)\mathsf{V}^{-1} \\ \mathsf{V} &= \begin{pmatrix} \sin^{-1/2}(2\pi\nu) & 0 \\ \frac{\cos(2\pi\nu)}{\sin^{1/2}(2\pi\nu)} & \sin^{1/2}(2\pi\nu) \end{pmatrix}. \end{aligned} \tag{A2}$$

The transformation is singular at $\nu = 0$.

Gumoski's maps

The maps considered in [4, 9] are

$$\left.\begin{aligned} x' &= y + F(x) \\ y' &= -x + F(x') \end{aligned}\right\} \qquad F(x) = \mu x + (1-\mu) f(x). \tag{A3}$$

Where $f(x) = x^2$, $x^2\mathrm{e}^{-(x^2-1)/4}$, $x^2/(1+x^2)$. The fixed points are given by $x = f(x)$ and the origin is elliptic if $|\mu| \leqslant 1$. Setting $\mu = \cos(2\pi\nu)$ the eigenvalues are $\mathrm{e}^{\pm \mathrm{i}2\pi\nu}$ and the conjugation of the linear part L into a rotation is given by

$$\mathsf{L} = \begin{pmatrix} \mu & 1 \\ \mu^2 - 1 & \mu \end{pmatrix} = \mathsf{V}\mathsf{R}(2\pi\nu)\mathsf{V}^{-1} \qquad \mathsf{V} = \begin{pmatrix} \sin^{-1/2}(2\pi\nu) & 0 \\ 0 & \sin^{1/2}(2\pi\nu) \end{pmatrix}. \tag{A4}$$

Setting, for brevity, $s = \sin(2\pi\nu)$, $c = \cos(2\pi\nu)$, the map written in the coordinates $\mathrm{x} = s^{1/2}x$, $\mathrm{y} = s^{1/2}y$ after the transformation V^{-1} reads

$$\begin{pmatrix} \mathrm{x}' \\ \mathrm{y}' \end{pmatrix} = \mathsf{R}(2\pi\nu)\begin{pmatrix} \mathrm{x} \\ \mathrm{y} \end{pmatrix} + (1-c)\begin{pmatrix} s^{1/2} f(\mathrm{x}s^{-1/2}) \\ cs^{-1/2} f(\mathrm{x}s^{-1/2}) + s^{-1/2} f(\mathrm{x}'s^{-1/2}) \end{pmatrix}. \tag{A5}$$

The transformation is singular even in this case, and the nonlinear part is affected by ν-dependent factors. The structure of this map is similar to maps obtained by writing the contribution of the nonlinear term $\mathsf{N} = \binom{x}{y+f(x)}$ and of the one-turn map as $\mathsf{N}^{1/2}\mathsf{L}\mathsf{N}^{1/2}$, whereas map (2) corresponds to $\mathsf{L}\mathsf{N}$, and we have set $\mathsf{N}^{1/2} = \binom{x}{y+f(x)}$.

References

[1] Hénon M 1969 *Q. Appl. Math.* **17** 291
[2] Bazzani A, Servizi G, Todesco E and Turchetti G A 1994 normal form approach to the theory of nonlinear betatronic motion *CERN Yellow Report* 94–02
[3] Bazzani A, Giovannozzi M, Servzi G, Todesco E and Turchetti G 1993 *Physica* D **64** 66
[4] Gumowski I 1972 Some properties of large amplitude solutions of conservative systems: part 1 quadratic and cubic nonlinearities *CERN/SI/Int.* BR/72-1
Gumowski I and Mira C 1980 *Dynamique Chaotique, Transformations Ponctuelles* (Toulouse: Cepadues Editions)
[5] Bountis A 1981 *Physica* D **3** 577
[6] Polymilis C, Servizi G and Skokos C 1997 *Celest. Mech. Dynam. Astron.* **66** 365
[7] Benettin G, Galgani L and Giorgilli A 1980 *Nuovo Cimento Lett.* **29** 163
[8] Month M and Herrera J C (ed) 1979 *Nonlinear Dynamics and the Beam–Beam interaction (Proc. AIP Conf. vol 57)* (New York: AIP)
[9] Gumowski I 1972 Some properties of large amplitude solutions of conservative systems: part 2 bounded nonlinearities *CERN/SI/Int.* BR/72-1
[10] Nusse H and Yorke J 1994 *DYNAMICS: Numerical Explorations* (Berlin: Springer)
[11] Servizi G, Bortolotti D, Todesco E, Giovannozzi M and Vrahatis M N 1995 *Int. J. Mod. Phys.* **6** 651
[12] Contopoulos G 1983 *Physica* D **8** 142
[13] Contopoulos G 1983 *Nuovo Cimento Lett.* **37** 1491
[14] Polymilis C and Hizanidis K 1993 *Phys. Rev.* E **47** 43
[15] Hénon M 1965 *Ann. Astrophys.* **28** 992
[16] Contopoulos G 1970 *Astron. J.* **75** 108
[17] Contopoulos G and Polymilis C 1993 *Phys. Rev.* E **46** 1546